FMFP2022-1300

Implementation of the Accurate Conservative Phase Field Method for two-phase incompressible flows in a finite volume framework

Sahaj S Jain¹, and Danesh Tafti²

¹ Engineering Mechanics, Department of Biomedical Engineering and Mechanics, Virginia Polytechnic Institute and State University, Virginia-24060, United States of America

²Department of Mechanical Engineering, Virginia Polytechnic Institute and State University, Virginia-24060, United States of America

ABSTRACT

The phase field method provides a simple mass conserving method for solving two-phase immiscible - incompressible Navier-Stokes Equations. The relative ease in implementing this method compared to other interface reconstruction methods, coupled with its conservativeness and boundedness makes it an attractive alternative. We implement the method in a parallel structured multi-block generalized coordinate finite volume solver using a collocated grid arrangement within the framework of the fractional-step method. The discretization uses a second-order central difference method for both the Navier-Stokes and the phase field equations. A TVD-based averaging technique is used for calculating density at cell faces in the pressure correction step to handle high-density ratios. The simulation framework is verified in standard test cases: Zalesak Disk, a droplet in shear flow, Solitary Wave Runup, Rayleigh Taylor Instability, and the Dam Break Problem. A second-order rate of convergence and excellent phase volume conservation is observed.

Keywords: Multiphase Flows, Diffused Interface Method, Phase Field Method, Finite Volume Method, Computational Fluid Dynamics

1. INTRODUCTION

The development of computational fluid dynamics tools for multiphase flows has found many applications in recent times, including, but not limited to large-scale flows such as wave-energy harvesting [1–4], to flows at much smaller scales such as droplet impact on surfaces [5–7].

While many methods exist, one-fluid methods such as the Diffused Interface Method are considered in this paper. The Diffused Interface Methods involve discretizing the domain into two different phases using a phase variable ϕ , which varies smoothly but sharply over the interface. The material properties, such as viscosity and density, are then interpolated from the phase field. These methods are typically categorized either as, Level Set Methods, or Phase Field Methods. While the Level Set Method involves a re-initialization step [8–10] which often results in a loss of accuracy, the Phase Field Method does not need a re-initialization step; instead, the phase convection and restoration are done at the same time. Typically, either Cahn-Hillard [11] or Allen-Cahn [12] equations are used

to solve for the phase. However, both have their disadvantages. The Cahn-Hillard equation, while being mass conserving, involves solving for fourth-order terms, whereas the Allen-Cahn equation, which only has second-order terms, is not mass conserving in nature.

Chiu and Lin [13] formulated the conservative phase field based on the conservative level set method [10] as follows:

$$\frac{D\phi}{Dt} = \gamma \nabla \cdot \left(\epsilon \nabla \phi - \phi (1 - \phi) \frac{\nabla \phi}{|\nabla \phi|} \right), \tag{1}$$

where $D(\cdot)/Dt$, is the material derivative, ϵ represents interface width, and γ , the reinitialization parameter is representative of the strength of the right-hand-side of equation (1), responsible for reinitializing and maintaining a hyperbolic tangent profile for the interface:

$$\phi = \frac{1}{2} \left(1 + \tanh\left(\frac{\psi}{2\epsilon}\right) \right) \tag{2}$$

where ψ is the signed distance function varying which represents distance normal to the interface such that $\psi(\phi=0.5)=0$. While the knowledge of the hyperbolic tangent profile is derived from the thermodynamics of the interface, thermodynamics plays no further role in the mechanics of the advection of the phase field [13,14]. The right-hand side, which contains a diffusion and an anti-diffusion term, for the hyperbolic tangent profile cancel each other out, ensuring that the phase is convected only by the flow.

Material properties θ (such as density and viscosity) can be derived from ϕ as

$$\Theta(x, y, z, t) = \Theta_0 \phi(x, y, z, t) + (1 - \phi(x, y, z, t))\Theta_1$$
(3)

where θ_1 correspond to material properties for the phase given by $\phi = 1$ and θ_0 correspond to material properties for the phase given by $\phi = 0$.

The conservative phase field method, which can be considered to be the one-step version of the conservative level set method of Olsson and Kreiss [10], requires no pseudo time marching, has been shown to have excellent conservative [13] and boundedness properties [14], is easy to implement and has been shown to have lower computational costs than the, otherwise more accurate Volume of Fluid Method (VOF) for cases where the interface spans the entire domain [15].

However, it has been observed that the conservative phase field method introduces artificial distortions in the interface [16]. S. S. Jain [17] reformulated the anti-diffusion term in (1),

using the signed distance function to introduce the *Accurate Conservative Phase Field Method (ACPF)*:

$$\frac{D\phi}{Dt} = \gamma \nabla \cdot \left(\epsilon \nabla \phi - \frac{1}{4} \left(1 - \tanh^2 \left(\frac{\psi}{2\epsilon} \right) \right) \hat{\boldsymbol{n}} \right) \tag{4}$$

Since ψ varies linearly with the distance, as compared to the phase which has a sharp variation across the interface it becomes more convenient to calculate the normal vector field in terms of the signed distance function:

$$\widehat{\boldsymbol{n}} = \frac{\boldsymbol{\nabla}\phi}{|\boldsymbol{\nabla}\phi|} = \frac{\boldsymbol{\nabla}\psi}{|\boldsymbol{\nabla}\psi|} \tag{5}$$

The signed distance function can be obtained analytically from the phase:

$$\psi = ln \left(\frac{\tilde{\phi} + \alpha}{1 - \tilde{\phi} + \alpha} \right) \tag{6}$$

where α is a very small number $(10^{-50}$ in this paper) introduced to avoid 0 in the numerator, $\tilde{\phi} = max((\alpha, \phi), 1 - \alpha)$, to limit the phase value within bounds. Further, the expression inside the bracket is constrained between α and $1/\alpha$ to avoid the calculations getting out of bounds.

The Accurate Conservative Phase Field Method has been shown to be more accurate than the Conservative Phase Field method and demonstrates better boundedness and reduced truncation error for the calculation of the curvature [17].

2. METHODOLOGY

2.1 Accurate Phase Field Method

The Accurate Conservative Phase Field Method is solved in a collocated grid framework using the second-order Adams-Bashforth algorithm for time marching. The domain is first initialized using ones and zeros for the phase and then the phase field method solver is run to initialize the diffused phase field. The diffusion and convection terms are treated in a finite volume framework where, while the diffusion term is treated using the second-order central difference method, numerous schemes are available in the house code GenIDLEST for the treatment of the convection term, including second-order central difference, QUICK scheme, and TVD flux limiters. The anti-diffusion term is treated using the second-order central difference method in a finite difference framework and the reinitialization parameter (γ) is updated every timestep as γ = $\gamma^* u_{max}$ [13–15,17], with a minimum value established as $\gamma =$ $0.1\gamma^*u_{ref}$, where γ^* is a constant factor (typically chosen to be 1.0), u_{max} is the maximum velocity in the field, and u_{ref} is the reference velocity.

While a boundedness criterion has been well established by Mirjalili et. al. [14], as a contingency, the phase is bounded by the limits $[\alpha, 1]$ to avoid any unforeseen division by zero errors, and the following treatment is provided to ensure phase volume conservation:

- 1. Calculate $\phi_d = \phi(1 \phi)$ for each node.
- 2. Calculate Phase Volume:

$$V(t) = \int_{\Omega} \phi d\Omega \tag{7}$$

Where Ω is the volume of the domain, and phase volume difference:

$$\Delta V(t) = V(t=0) - V(t) \tag{8}$$

3. Apply the correction:

$$\phi^c = \phi + \frac{\Delta V \phi_d}{\int_{\Omega} \phi_d d\Omega} \tag{9}$$

This can be considered to be a first-order operation in moving the interface uniformly throughout the domain by a distance dL in the normal direction to incur a ΔV change in phase volume.

2.2 Conservation of Mass and Momentum

The dynamics of two-phase incompressible immiscible flows are determined by the incompressible Navier-Stokes Equations:

$$\nabla \cdot \boldsymbol{u} = 0 \tag{10}$$

$$\rho\left(\frac{\partial \boldsymbol{u}}{\partial t} + \boldsymbol{\nabla} \cdot (\boldsymbol{u}\boldsymbol{u})\right) = -\boldsymbol{\nabla}p + \boldsymbol{\nabla} \cdot (\mu \boldsymbol{\nabla}\boldsymbol{u}) + \rho \boldsymbol{g}, \tag{11}$$

where p is pressure, u is the velocity, g is the acceleration due to gravity, and density (ρ) & dynamic viscosity (μ) are approximated using equation (3). Capillary forces have been neglected in this paper.

These simulations are performed using the in-house FVM CFD code Generalized Incompressible Direct and Large Eddy Simulation of Turbulence (GenIDLEST) [18] using the fractional step method. A collocated grid framework is adopted where phase, the signed distance function, velocity, pressure, density, and viscosity are stored at cell centers and a fully explicit second-order Adams-Bashforth algorithm is adopted for time marching. At each time step, the following steps are performed:

- 1. Predict a velocity field u^* using the momentum equation and interpolate to cell faces to calculate cell face fluxes c using the available pressure field, p_0 .
- 2. Solve for the phase using the following steps:
 - a. Calculate the signed distance function ψ and the term $\mathbf{S} = \frac{1}{4} \left(1 \tanh^2 \left(\frac{\psi}{2\epsilon} \right) \right) \hat{\mathbf{n}}$ at cell centres. Calculate the divergence of \mathbf{S} to obtain the source term
 - b. Use cell face velocity fluxes to calculate the convection term and use second-order central difference to obtain the diffusion term.
 - c. Find the new phase values by using the 2^{nd} order Adams-Bashforth Method. Adjust the phase between the limits $[\alpha, 1]$ and apply the correction for phase volume conservation. Update density and viscosity.
- 3. Use u^* interpolate to cell faces to calculate cell face fluxes c^* .
- 4. Using predicted cell face flux values c*, calculate pressure correction with the variable coefficient Poisson equation using a preconditioned BICG-STAB solver:

$$\nabla \cdot \left(\frac{1}{\rho} \nabla (p' \Delta t)\right) = \nabla \cdot c^* \tag{12}$$

5. Update the pressure as $p = p_0 + p'$, where p_0 is the pressure at the previous timestep. Use the pressure correction to update the velocity, \boldsymbol{u} , field, and the cell face velocity fluxes, \boldsymbol{c} .

3. VALIDATION AND VERIFICATION

Five generic test cases were considered for numerical verification of the phase field method:

- a. Droplet in Shear flow
- b. Zalesak Disk
- c. Rayleigh Taylor Instability
- d. Solitary Wave
- e. Dam Break Problem

The first two are the standard test cases for evaluating advection schemes [19] whereas the latter involves solving the full Navier-Stokes coupled with the Phase Field Method.

3.1 Droplet in Shear Flow

In this standard test case introduced by Rider and Kothey [20], a droplet of radius 0.15 is introduced at the position (0.50,0.75) in the domain of $[0,1] \times [0,1]$ with a prescribed velocity field given by the following stream function:

$$\psi = \frac{1}{\pi} \sin^2(\pi x) \sin^2(\pi y) \cos(\pi t/T) \tag{13}$$

where T = 4.

The droplet is allowed to deform as much as possible and at t = T/2, the velocity field is reversed, and the circular droplet is restored. The initial and final shapes are compared to calculate the shape error as:

Shape
$$Error = \sum_{i,j} |\phi_{t=0}(i,j) - \phi_{t=T}(i,j)| \Delta x \Delta y$$
 (14)

Five simulations for grid sizes 32×32 , 64×64 , 128×128 , 256×256 , and 512×512 were performed with the parameters $\epsilon = 1.0 \Delta x$, $\gamma = 1.0 u_{max}$ using both the Conservative Phase Field (CPF) and Accurate Conservative Phase Field Method (ACPF). The shape errors were compared with the results of S. S. Jain [17] and a near second-order rate of convergence, comparable to previous studies (Figure 1) is observed. It is also observed that the Accurate Phase Field Method is more accurate than the Conservative Phase Field Method (Table 1). The final shapes were also visually compared for different grid sizes (Figure 2) to the exact solution and convergence is observed for higher resolutions.

Table 1: Shape Error comparison for Droplet in Shear Flow test case between Conservative Phase Field (CPF) and Accurate Conservative Phase Field (ACPF) methods

Grid Size	Δt	Shape Error	
		CPF	ACPF
32 × 32	2.00e-3	5.23E-02	5.43E-02
64×64	1.00e-3	1.63E-02	1.40E-02
128×128	5.00e-4	3.74E-03	3.57E-03
256×256	2.50e-4	1.11E-03	8.66E-04
512×512	1.25e-4	4.37E-04	2.88E-04

3.2 Zalesak Disk

In this standard test case introduced by Zalesak [21], a circular disk of radius 15 with a notch of width 5 and height 25 is introduced at the position (50,75) in the domain of $[0,100] \times [0,100]$ with a prescribed rigid body velocity field:

$$[0,100] \times [0,100]$$
 with a prescribed rigid body velocity field:
 $u_x = \pi \frac{50 - y}{314}$, $u_y = \pi \frac{x - 50}{314}$ (15)

We set $\epsilon = 0.7 \Delta x$, $\gamma = 2.5 u_{max}$. The problem is non-dimensionalized with $l_{ref} = 100.0$ and $u_{ref} = 1.0$. This test

case is used to test the ability to preserve sharp corners; the slotted disk should be convected as it is by the flow field undergoing minimal possible deformations [19]. The initial and final shapes at T=0 and T=628 are compared in **Figure 3** for grid sizes 128x128, 256x256 and 512×512 , with $\Delta t=0.064$ Δx and it is observed that higher resolutions are able to preserve the sharp corners better.

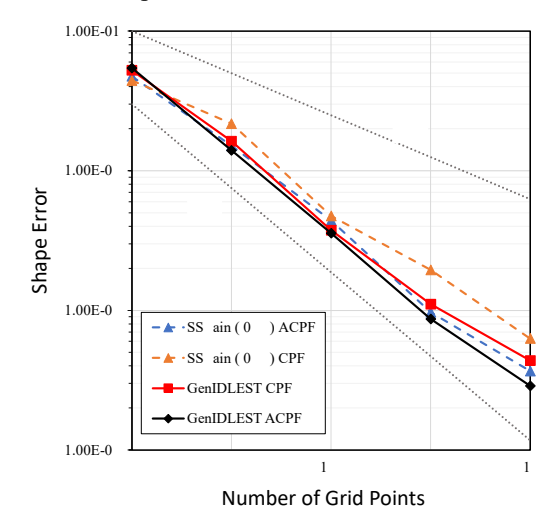


Figure 1: Shape Errors for Droplet in Shear Flow test case

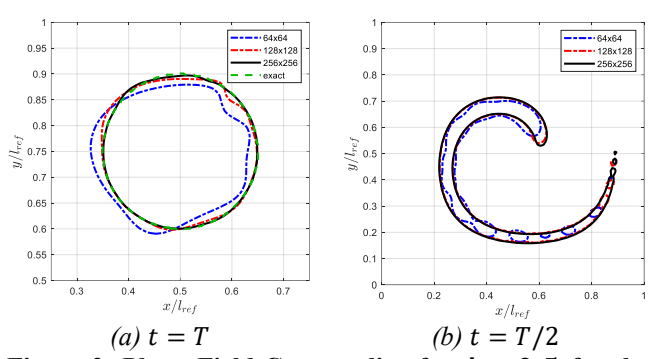


Figure 2: Phase Field Contour line for $\varphi=0.5$ for the Droplet in Shear Flow test case

3.3 Rayleigh Taylor Instability

The first dynamic test case considered is the evolution of Rayleigh Taylor instability for low Atwood numbers. Such instability occurs due to the action of gravitational forces when a heavier fluid sits on top of a lighter fluid.

The domain $[0,D] \times [-2D,2D]$ is filled with two fluids in equal volumes of density ratio prescribed by Atwood number $At = (\rho_1 - \rho_0)/(\rho_1 + \rho_0) = 0.5$, and equal viscosity. For the phase, we use, $\gamma^* = 1.0$ and $\epsilon = 2.0\Delta x$. The interface is located at $y(x) = 0.1D\cos(2\pi x/D)$. The reference velocity is $u_{ref} = \sqrt{gD}$ and time is non-dimensionalized using $t_{ref} = D/u_{ref}$. The Reynolds number is $Re = \rho_1 u_{ref} D/\mu = 3000$, the Froude Number is $Fr = u_{ref}/\sqrt{gD} = 1$ and surface tension forces are neglected. No-slip boundary conditions are used on the top and bottom walls and periodic boundary conditions are used on the left and right sides of the domain.

We studied this case for two grid sizes 200×800 and 400×1600 . These simulations were performed in a multi-

block framework, with 16 blocks stacked over each other in the \hat{y} direction.

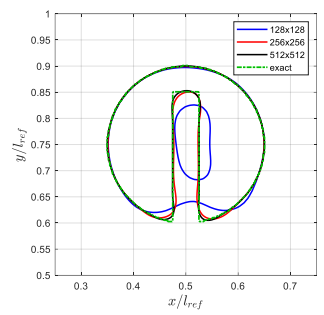


Figure 3: Zalesak Disk: Final Shape for grid sizes 128x128, 256x256 and 512×512

The phase contour profile for the evolution of the instability is given in **Figure 5**. We also compare the y-coordinates of the top and bottom of the interface with previously performed numerical simulations [13,22,23] and good agreement is observed, as seen in **Figure 4**. Here, the time is non-dimensionalized using Atwood Number, as $t^* = (t/t_{ref})\sqrt{(At)}$.

3.4 Solitary Wave Run-up

This test case is used to quantify the effects of viscous damping and study the interaction of the interface with solid walls for high-density ratios. In a 2-dimensional domain $[-h, h] \times [0,20h]$, the water free surface is prescribed using the following elevation profile:

$$A(x, t = 0) = \frac{A_0}{\cosh^2(x\sqrt{0.75A_0})}$$
 (16)
We use $h = 0.1 \, m$, and the theoretical wave speed is $C_w =$

We use h=0.1~m, and the theoretical wave speed is $C_w=\sqrt{gh}=1~m/s$. We use $g=10m/s^2$ for the sake of convenience. The density and viscosity of water and air are prescribed as $\rho_a=1.2~kg/m^3$, $\mu_a=1.8e-05~Pa.s$, $\rho_w=1000~kg/m^3$ and $\mu_w=1.0e-03~Pa.s$, the Reynolds number is $Re=\rho_w C_w h/\mu_w=1.0\times 10^5$ and the Froude number is $Fr=u_{ref}/\sqrt{gh}=1$.

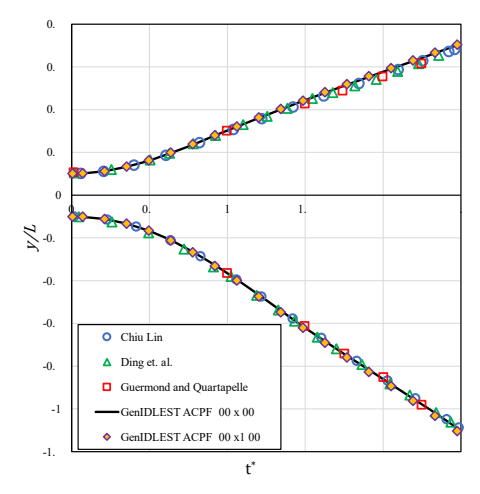


Figure 4: The evolution of the y-coordinate of the top and bottom of the interface with time for Rayleigh Taylor Instability.

A grid of 400×200 is employed with a fixed time step size $\Delta t/t_{ref} = 1.0 \times 10^{-4}$. These simulations were performed on 25 blocks in the \hat{x} direction. For the phase, $\gamma^* = 1.0$ and $\epsilon = \sqrt{A_{cell}}$ is used. TVD flux limiters are used to calculate the density cell face values for pressure correction. **Figure 6** depicts the evolution of the solitary wave for $A_0/h = 0.5$. For $A_0/h = 0.5$, a maximum phase volume change of $|\Delta V/V_0| \approx 5.15 \times 10^{-6}$ % is observed, and the wave speed is ~ 1.0625 m/s, which is close to the theoretical wave speed.

We first study the wave run-up height (A_{runup}) as a function of the wave amplitude when the wave is at x = 10 (A_c) in **Figure 7**. The results compare favourably against both, previously performed numerical simulations [24,25], and the experiment by Chan and Street [26].

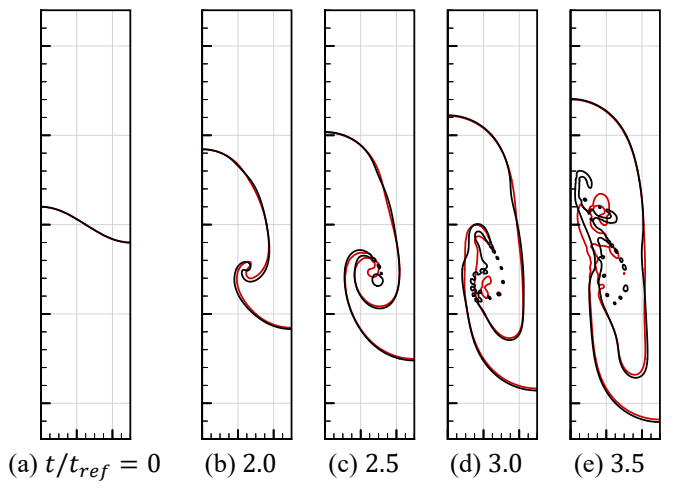


Figure 5: The evolution of the interface for Rayleigh Taylor instability for grid sizes 400×1600 (black) and 200×800 (red)

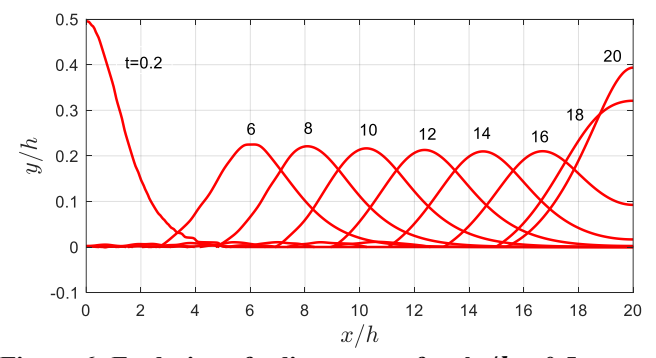


Figure 6: Evolution of solitary wave for $A_0/h = 0.5$

We also study the viscous damping effects, by comparing the evolution of wave amplitude for $A_0/h = (0.1, 0.3, 0.5, 0.7, 0.9)$, starting from $t/t_{ref} = 6$ (when the wave is free from the wall) to $t/t_{ref} = 14$, with the analytical solution predicted by Mei et al [27]:

$$A_{max}^{-1/4} = A_{0max}^{-1/4} + 0.08356 \frac{C_w t^*}{h} \sqrt{\left(\frac{1}{Reh^{1/2}}\right)}$$
 (17)

where A_{0max} is the wave amplitude at $t/t_{ref} = 6$, $t^* = t - 6t_{ref}$ and A_{max} is the wave amplitude. The numerical solutions show good agreement with the perturbation solutions for low

values of A_{0max} (**Figure 8**) while higher viscous damping is observed for higher amplitudes; this is expected as the small amplitude approximation is only valid for $A_{0max}/h \le 0.1$.

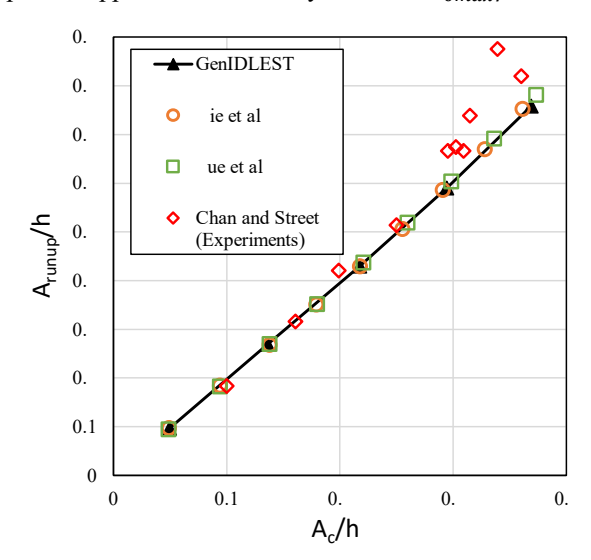


Figure 7: Wave run-up versus wave amplitude when the wave is at x/h = 10

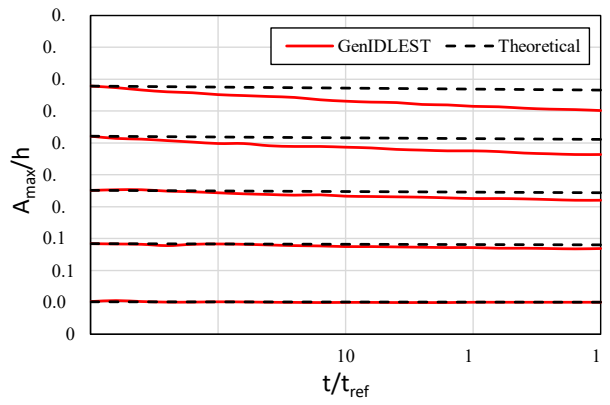


Figure 8: Evolution of wave amplitude versus time to quantify viscous damping effects

3.5 Dam Break Problem

This free surface problem involves simulating the collapse of the water column. A water column of height 2L and width L is prescribed in the bottom left corner of the domain: $[0,4L] \times [0,4L]$. The same material properties as in the solitary wave example are used, surface tension forces are neglected and acceleration due to gravitation is $g=-9.81m/s^2$. L=0.146~m is used as a reference length, $u_{ref}=\sqrt{g(2L)}=1.6295~m/s$ is used as a reference velocity which leads to the Reynolds Number $Re=\rho_w u_{ref}L/\mu_w\approx 2.38\times 10^5$ and the Froude Number $Fr=u_{ref}/\sqrt{gL}\approx 1.414$. For the phase, $\gamma^*=1.0$ and $\epsilon=4.0\Delta x$ is used.

TVD flux limiters are employed to calculate convective terms in both, phase and momentum equations, and density cell face values and a no-slip boundary condition are applied to all the domain boundaries. The simulation is first performed for a two-dimensional uniform grid of size 600×600 with a fixed time step size $\Delta t/t_{ref} = 2.5 \times 10^{-5}$.

This simulation was repeated on a non-uniform grid of size 400×400 with the grid refined to $\Delta x = 2L/600$ at the left, right, and the bottom walls, with a fixed time step size $\Delta t/t_{ref} = 0.625 \times 10^{-5}$. For the phase, $\gamma^* = 1.0$ and $\epsilon = 7.6808 \sqrt{min(A_{cell})}$ is used. Both simulations were performed on 25 blocks (5 in each direction). We compare the position of the surge front versus time for both the simulations with previously performed numerical simulations [13,28] and experiments [29,30] and a good agreement is observed as seen in **Figure 9**.

A maximum phase volume change of $|\Delta V/V_0| \approx 5.06 \times 10^{-4}$ % and 9.23×10^{-3} % was observed for the uniform and non-uniform grids respectively between t=0 and $t=4t_{ref}$.

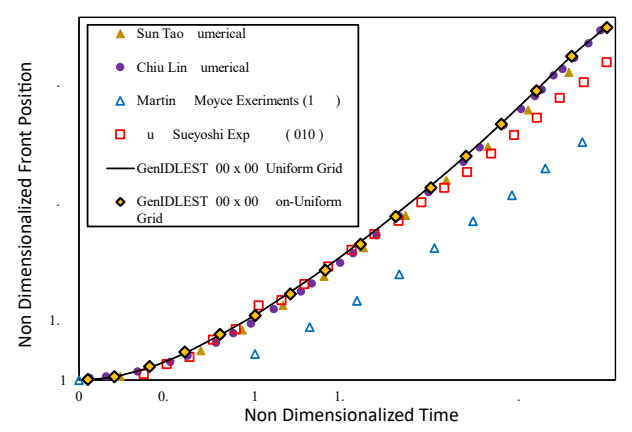


Figure 9: Evolution of the wave front position of the collapsing water column with time

4. CONCLUSION

We implemented the Accurate Conservative Phase Field Method in a Finite Volume parallel multi-block collocated grid framework, and with the help of the droplet in shear flow test case and observed that it is more accurate than the Conservative Phase Field Method. The implementation was also verified against standard test cases such as Zalesak Disk, Rayleigh Taylor Instability, Solitary Wave, and the Dam Break Problem, and showed good agreement with theoretical, experimental, and previously performed numerical results. The method shows excellent phase volume conservativeness, even in cases where we have very high-density ratios.

ACKNOWLEDGEMENTS

We would like to thank the Virginia Tech ARC (Advanced Research Computing) for providing the computational resources required for this work.

NOMENCLATURE

φ	Phase	
ψ	Signed Distance Function	[m]
ϵ	Interface Width Parameter	[m]
γ	Reinitialization Parameter	[m/s]
γ^*	Scaled Reinitialization Parameter	
\boldsymbol{V}	Gradient Operator	[1/m]
$\boldsymbol{\varTheta}$	Material Properties	
ñ	Normal Vector Field	

V(t)	Phase Volume	$[m^3]$
u	Velocity	[m/s]
p	Pressure	[Pa]
ρ	Density	$[kg/m^3]$
μ	Dynamic Viscosity	[Pa.s]
g	Acceleration due to gravity	$[m/s^2]$
At	Atwood Number	
Re	Reynolds Number	
Fr	Froude Number	

REFERENCES

- [1] Khedkar, K., and Bhalla, A. P. S., 0, "A Model Predictive Control (MPC)-Integrated Multiphase Immersed Boundary (IB) Framework for Simulating Wave Energy Converters (WECs)," Ocean Eng., 260, p. 111908
- [2] Benites-Munoz, D., Huang, L., Anderlini, E., Marín-Lopez, . R., and Thomas, G., 0 0, "y drodynamic Modelling of An Oscillating Wave Surge Converter Including Power Take-Off," . Mar. Sci. Eng., 8(10), p. 771.
- [3] Schmitt, P., and Elsaesser, B., 01, "On the Use of OpenFOAM to Model Oscillating Wave Surge Converters," Ocean Eng., 108, pp. 98–104.
- [4] Wei, . , Rafiee, A., en ry, A., and Dias, F., 01, "Wave Interaction with an Oscillating Wave Surge Converter, Part I: Viscous Effects," Ocean Eng., 104, pp. 185–203.
- [5] Luo, L., Wang, X.-P., and Cai, X.-C., 01, "An Efficient Finite Element Method for Simulation of Droplet Spreading on a Topologically Rough Surface," . Comput. Phys., **349**, pp. 233–252.
- [6] Yada, S., Lacis, U., van der Wijngaart, W., Lundell, F., Amberg, G., and Bagheri, S., 0, "Droplet Impact on Asymmetric y drophobic Microstructures," Langmuir, **38**(26), pp. 7956–7964.
- [7] Zhang, Q., Qian, T.-Z., and Wang, X.-P., 01, "Phase Field Simulation of a Droplet Impacting a Solid Surface," Phys. Fluids, **28**(2), p. 22103.
- [8] Sussman, M., and Smereka, P., 1, "Axisymmetric Free Boundary Problems," . Fluid Mech., **341**, pp. 269–294.
- [9] Sethian, . A., and Smereka, P., 00, "L EVEL S ET M ETHODS FOR F LUID I NTERFACES," Annu. Rev. Fluid Mech., **35**(1), pp. 341–372.
- [10] Olsson, E., and Kreiss, G., 00, "A Conservative Level Set Method for Two Phase Flow," . Comput. Phys., 210(1), pp. 225–246.
- [11] Cahn, . W., and illiar d, . E., "Free Energy of a o nuniform System. I. Interfacial Free Energy," p. 11.
- [12] Allen, S. M., and Cahn, . W., 1 , "A Microscopic Theory for Antiphase Boundary Motion and Its Application to Antiphase Domain Coarsening," Acta Metall., 27(6), pp. 1085–1095.
- [13] Chiu, P.-H., and Lin, Y.-T., 011, "A Conservative Phase Field Method for Solving Incompressible Two-Phase Flows," . Comput. Phys., **230**(1), pp. 185–204.
- [14] Mirjalili, S., Ivey, C. B., and Mani, A., 0 0, "A Conservative Diffuse Interface Method for Two-Phase

- Flows with Provable Boundedness Properties," Comput. Phys., **401**, p. 109006.
- [15] Mirjalili, S., Ivey, C. B., and Mani, A., 2019, "Comparison between the Diffuse Interface and Volume of Fluid Methods for Simulating Two-Phase Flows," Int. J. Multiph. Flow, **116**, pp. 221–238.
- [16] Jain, S. S., Adler, M. C., West, J. R., Mani, A., Moin, P., and Lele, S. K., 0 1, "Assessment of Diffuse-Interface Methods for Compressible Multiphase Fluid Flows and Elastic-Plastic Deformation in Solids."
- [17] ain, S. S., 0, "Accurate Conservative Phase-Field Method for Simulation of Two-Phase Flows," . Comput. Phys., **469**, p. 111529.
- [18] Tafti, D. K., 001, "GenIDLEST: A Scalable Parallel Computational Tool for Simulating Complex Turbulent Flows," Fluids Engineering, American Society of Mechanical Engineers, New York, New York, USA, pp. 347–356.
- [19] Prosperetti, A., and Tryggvason, G., eds., 2007, Computational Methods for Multiphase Flow, Cambridge University Press, Cambridge.
- [20] Rider, W., and Kothe, D., 1 , "Stretching and Tearing Interface Tracking Methods," 12th Computational Fluid Dynamics Conference, American Institute of Aeronautics and Astronautics.
- [21] Zalesak, 1 , "Fully Multidimensional Flux-Corrected Transport Algorithms for Fluids."
- [22] Ding, ., Spelt, P. D. M., and Shu, C., 00, "Diffuse Interface Model for Incompressible Two-Phase Flows with Large Density Ratios," . Comput. Phys., **226**(2), pp. 2078–2095.
- [23] Guermond, J.-L., and Quartapelle, L., 000, "A Projection FEM for Variable Density Incompressible Flows," . Comput. Phys., **165**(1), pp. 167–188.
- [24] Xie, Z., Stoesser, T., Yan, S., Ma, Q., and Lin, P., 2020, "A Cartesian Cut-Cell Based Multiphase Flow Model for Large-Eddy Simulation of Three-Dimensional Wave-Structure Interaction," Comput. Fluids, 213, p. 104747.
- [25] Yue, W., Lin, C.-L., and Patel, V. C., 00, "u merical Simulation of Unsteady Multidimensional Free Surface Motions by Level Set Method," Int. . u mer. Methods Fluids, 42(8), pp. 853–884.
- [26] Chan, R. K.-C., and Street, R. L., 1 0, "A Computer Study of Finite-Amplitude Water Waves," . Comput. Phys., 6(1), pp. 68–94.
- [27] Mei, C. C., Stiassnie, Michael., and Yue, D. K.-P., 2005, Theory and Applications of Ocean Surface Waves, World Scientific, Singapore;
- [28] Sun, D. L., and Tao, W. Q., 010, "A Coupled Volume-of-Fluid and Level Set (VOSET) Method for Computing Incompressible Two-Phase Flows," Int. . ea t Mass Transf., 53(4), pp. 645–655.
- [29] u, C., and Sueyoshi, M., 010, "u merical Simulation and Experiment on Dam Break Problem,". Mar. Sci. Appl., 9(2), pp. 109–114.
- [30] Martin, . C., and Moyce, W. ., 1 , "Part IV. An Experimental Study of the Collapse of Liquid Columns on a Rigid o rizontal Plane," Philos. Trans. R. Soc. Lond. Ser. Math. Phys. Sci., **244**(882), pp. 312–324.